THE EAS-TOP EXPERIMENT

G. Navarra[a,b,c] for the EAS-TOP Collaboration

May 19, 1999

[a] Dipartimento di Fisica Generale dell'Universita' di Torino, Italy
[b] Istituto Nazionale di Fisica Nucleare, Sezione di Torino, Italy
[c] Istituto di Cosmo-Geofisica del CNR, Torino, Italy

Abstract

The main aims and the characteristics of the EAS-TOP experiment at the Gran Sasso Laboratories are summarized. The results concerning the studies of the *knee* are reporteded; for other data the bibligraphy is quoted.

1 Introduction

The EAS-TOP array (Campo Imperatore, 2000 m a.s.l., above the underground Gran Sasso laboratories, see figs. 1, 2, 3) consists of:

- the e.m. detector (35 modules of scintillators, 10 m^2 each, 8 of them equipped with vertical scintillators in order to improve the response to Horizontal Air Showers), fully efficient for $N_e > 10^5$ [1,2];

- the muon-hadron detector (140 m^2 calorimeter with 9 layers of 13 cm iron absorbers and streamer tubes active elements, operating at $E_h > 50\ GeV$, and $E_\mu > 1\ GeV$) + 130 m^2 scintillator muon detectors distributed in the field (two vertical walls made of streamer tubes operate at the North and South sides of the detector to provide a trigger to nearly horizontal muons and to help in their reconstruction) [3];

- the Cherenkov light detector (8 telescopes with tracking capabilities equipped with imaging photomultipliers and wide angle optics) [4,5];

- three radio antennas for EAS radio emission measurements;

- moreover it operates in coincidence with the underground MACRO and LVD muon detectors ($E_\mu > 1.3\ TeV$; full area $A_\mu^{TeV} \approx 1000\ m^2$) [6-10].

Main aims of the experiment are of:

- contributing to construct the experimental knowledge of cosmic radiation in the energy range $10^{13} - 10^{17}$ eV (i.e. around the "knee" of the primary spectrum), through the available observables: spectra [11], composition [7,12], anisotropies [13,14], gamma-ray primaries [15-19];

- performing multiparametric analysis, which are essential for the debugging of the "interaction-composition-fluctuation" problem in the understanding of EAS data, through the interpretation of a subset of individual events [10];

- checking the main features of the high energy hadron interactions relevant for the interpretation, and the extrapolation to higher energies of the models elaborated from the accelerator data [10, 20, 21, 22];

- providing informations to interpret the deep underground data [10].

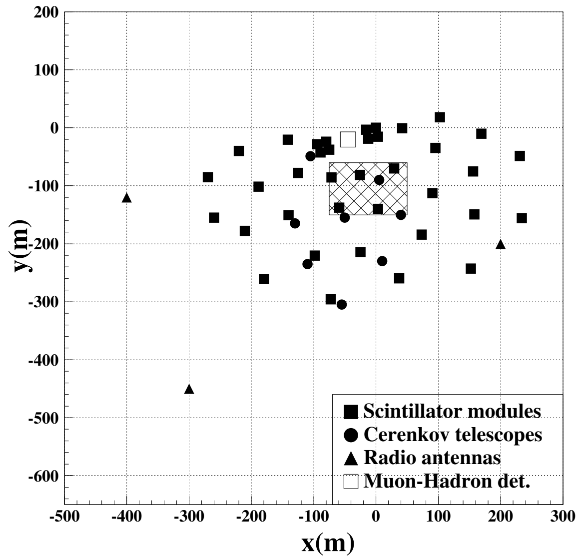

Figure 1: *The EAS-TOP array. The shaded area shows the core location region used for the shower size spectrum measurement.*

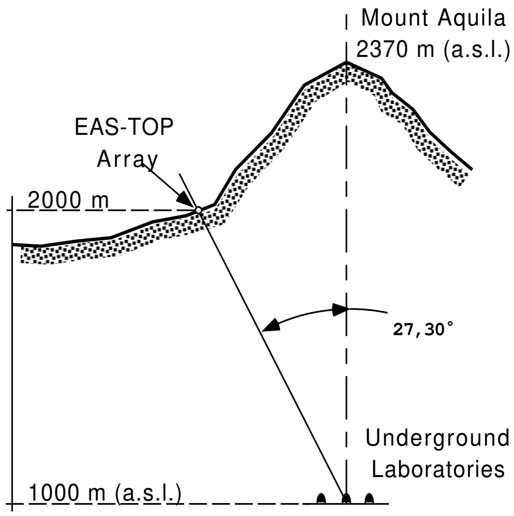

Figure 2: *The EAS-TOP array location with respect to the underground Gran Sasso laboratories.*

Table 1: *Results obtained from the fits to the Ne and $N\mu$ spectra measured in different bins of zenith angle (1,2 = below, above the knee).*

$\Delta \sec\theta$	γ_1	γ_2	$I(> Ne_k, N\mu_k) \times 10^7$ $m^{-2}s^{-1}sr^{-1}$	$Log(Ne_k, N\mu_k)$
e $1.00 - 1.05$	2.56 ± 0.02	2.99 ± 0.09	0.99 ± 0.2	6.09 ± 0.05
$1.05 - 1.10$	2.55 ± 0.02	2.93 ± 0.11	1.01 ± 0.3	6.02 ± 0.07
$1.10 - 1.15$	2.55 ± 0.03	2.85 ± 0.12	0.93 ± 0.4	5.97 ± 0.08
$1.15 - 1.20$	2.56 ± 0.03	2.81 ± 0.16	0.80 ± 0.4	5.93 ± 0.14
$1.20 - 1.25$	2.59 ± 0.03	2.91 ± 0.26	0.52 ± 0.3	5.95 ± 0.11
$1.25 - 1.30$	2.55 ± 0.07	2.80 ± 0.11	1.30 ± 0.6	5.63 ± 0.12
μ 1.00 - 1.05	3.12 ± 0.1	3.52 ± 0.1	1.0 ± 0.2	4.72 ± 0.1
1.10 - 1.15	3.07 ± 0.1	3.52 ± 0.1	0.7 ± 0.2	4.77 ± 0.1

2 The studies of the *knee*

Shower size spectra observed at different zenith angles in the region of the knee are shown in fig. 4. The break is observed at decreasing shower size with increasing atmospheric

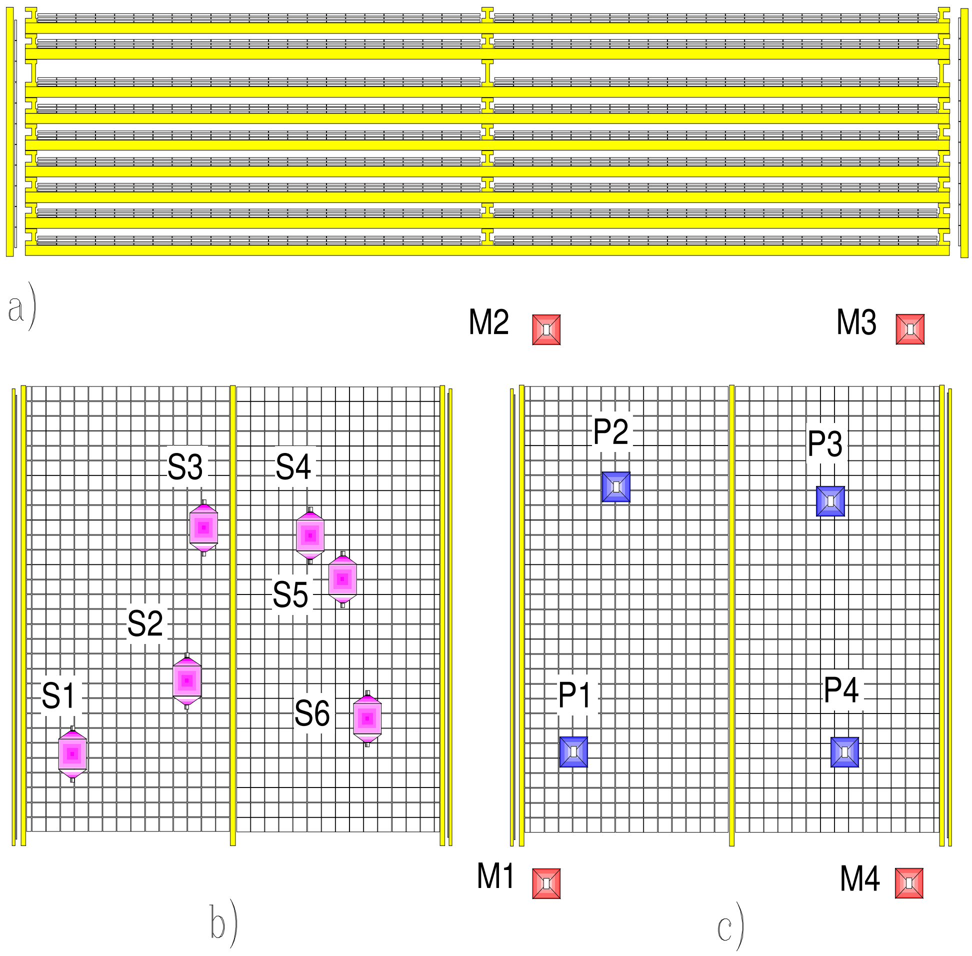

Figure 3: a) layout of the EAS-TOP calorimeter. The frame, the iron absorbers, the three layer chamber structure and the vertical walls are shown; b) 7th plane, top view, with the S scintillators set; c) 9th plane, top view, with the M and P scintillators, mainly used for triggering purposes.

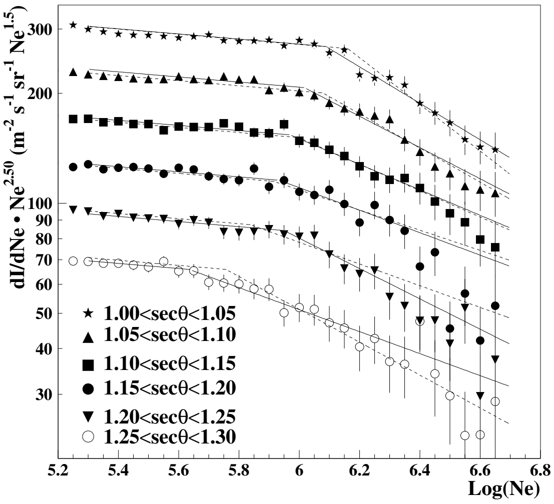

Figure 4: *Differential shower size spectra measured at different atmospheric depths. The solid lines show the results of the fitting procedure with 3 free parameters per spectrum; dashed lines those of the procedure requiring constant integral flux above the knee.*

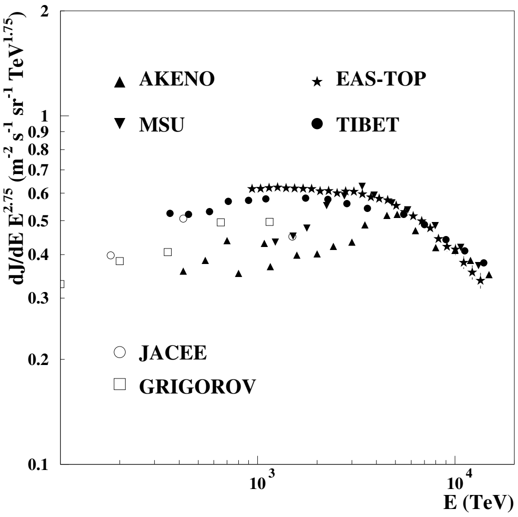

Figure 5: *The all particle energy spectrum obtained from the EAS-TOP shower size data, compared with the results of other experiments operating outside the atmosphere or at ground level.*

depth (i.e. zenith angle), and at constant intensity (see tab. 1). The absorbtion length of EAS particles at the knee (i.e. Ne_k) is $\Lambda_k = 220 \pm 3$ g cm^{-2}, in agreement with the measurements obtained from the "constant intensity cut" technique ($\Lambda_{EAS} = 217 \pm 3$ g cm^{-2}).

The all particle energy spectrum, as obtained from the conversion of the size spectrum, is shown in fig. 5 (the value of $< A >$ as resulting from the extrapolation of the direct measurements, and a rigidity dependent knee are used; all conversions and comparisons with expectations are performed by using the CORSIKA-HDPM model).

Muon number spectra as observed at two different atmospheric depths are shown in fig. 6 (N_μ^{GeV} being obtained from the reconstructed number of muon tracks in the muon-hadron detector). Further comparison of the knee parameters as measured in the e.m. and muon components at different atmospheric depths are shown in tab. 1, and in fig. 7 concerning the relation between the exponents of the N_e and N_μ^{GeV} spectra, which also demonstrate good consistency and agreement with the expectations from usual hadron interaction models.

The scatter plot of a sample of vertical and inclined (≈ 25 deg) events in the $N_e - {N_\mu}^{GeV}$ observables are shown in figs. 8 and 9. On the same plots, the position of the knee as independently identified in N_e and ${N_\mu}^{GeV}$ is shown. At both zenith angles (in agreement with consistent absorption properties of EAS at the knee), the knee error box is inside the distribution of the experimental points, far from the upper and lower edges, which

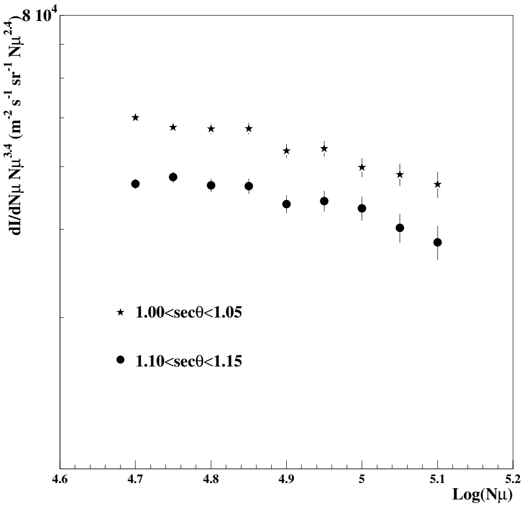

Figure 6: *N_μ spectra measured in two different intervals of zenith angles.*

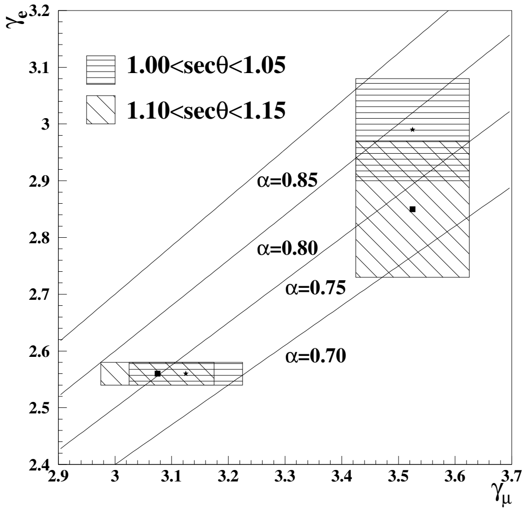

Figure 7: *Comparison of the slopes of the Ne and Nμ spectra measured below and above the knee: α is the index of the $N_e - N_\mu$ relation ($N_\mu \propto N_e^\alpha$).*

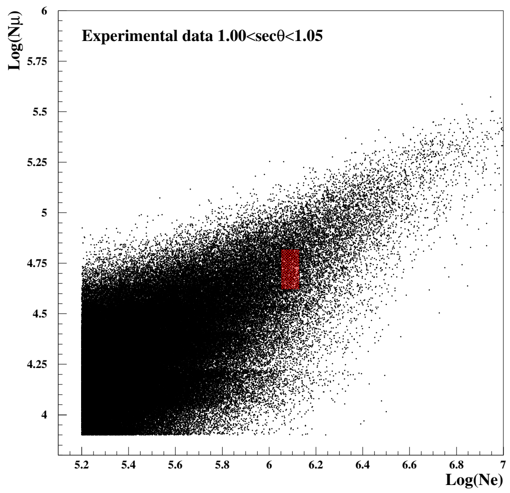

Figure 8: *Scatter plot of N_μ vs. N_e data for vertical events, with the identification of the knee in the two components shown.*

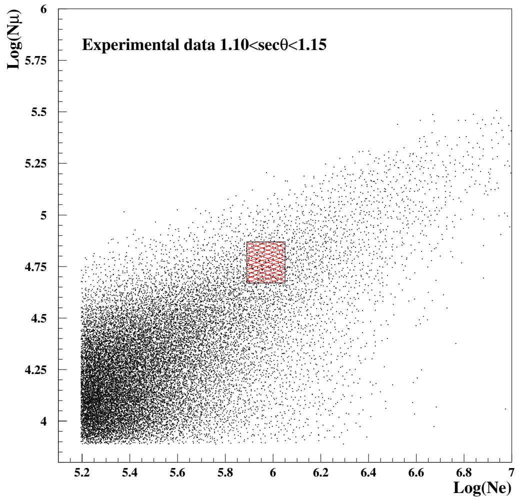

Figure 9: *Same as figure 8 for experimental data for $24.6° < \theta < 29.6°$.*

correspond to very heavy (iron) and light (proton) primaries, so that a break in such components is unlikely. Intermediate mass nuclei ("CNO-Helium like") are thus favoured.

For protons, He and CNO nuclei, the primary energies corresponding to $Ne_k = 1.2\ 10^6$, at the observation depth of $x = 820$ g cm^{-2} are respectively $E_O = (2.7 - 3.4 - 4.1)10^{15}$ eV. Values of $E_O \approx 4.\ 10^{15}$ eV (corresponding to the quoted "CNO-Helium like" primaries, best candidates to fit the break in N_e and $N_\mu{}^{GeV}$ data) agree with the energy determination of the knee from the TUNKA atmospheric Cherenkov detector (which is rather independent on the primary composition). Absolute intercalibrations of the detectors, and combined measurements could therefore be of main significance.

2.1 The composition around the *knee* : $e.m. + \mu$ detectors

The GeV muon content vs. the shower size is studied in the "knee" region, from the EAS-TOP muon detector data (the layout of the muon-hadron detector is shown in fig. 3). The muon lateral distribution in a given interval of shower size is shown in fig.10, together with the expectations from the CORSIKA-HDPM code and the mixed composition resulting from the extrapolation of the direct data. The same good fit is obtained for the $Ne - N_\mu$ relation shown in fig.11. Above the knee, a slightly heavier composition, as resulting from a rigidity-dependent knee seems favourite, but the contemporaneous check of the interaction model used and a larger statistics at larger shower sizes is necessary for a firm conclusion. The composition model reproduces as well the muon number fluctuations for fixed shower size in the different energy ranges.

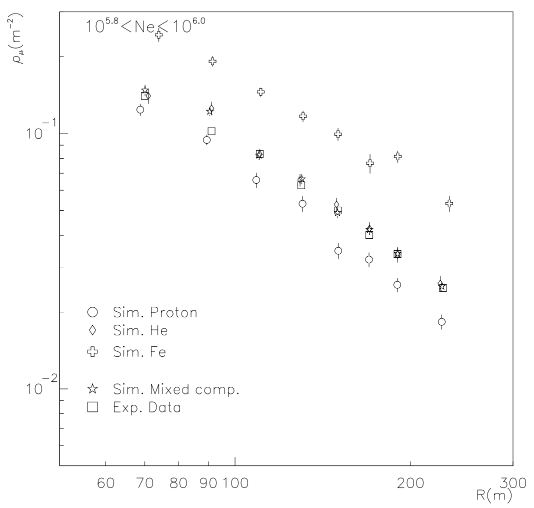

Figure 10: *Muon lateral distribution below the "knee".*

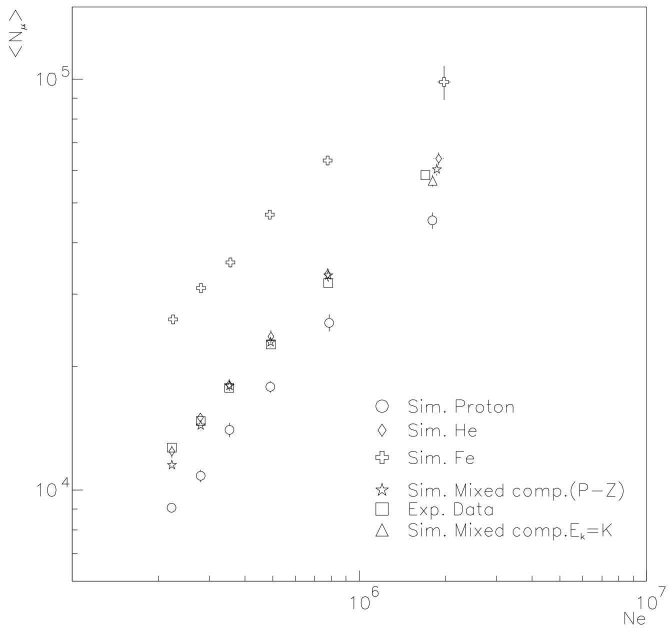

Figure 11: $< N_\mu > vs N_e$

2.2 The composition around the $knee$: $EAS-TOP$ and $MACRO$

In fig. 12 the muon ($E_\mu > 1.3\ TeV$) multiplicity distributions recorded by MACRO in two intervals of shower sizes, together with the expectations for different composition models around the knee: constant composition ($Ek(Z) = Ek(1)$), and rigidity dependent knee (e.g. Peters-Zatsepin model: $Ek(Z) = Z * Ek(1)$; with DPMJET interaction model) aree shown. The latter, although with a still limited statistics, seems favoured by the large multiplicity tail above the knee.

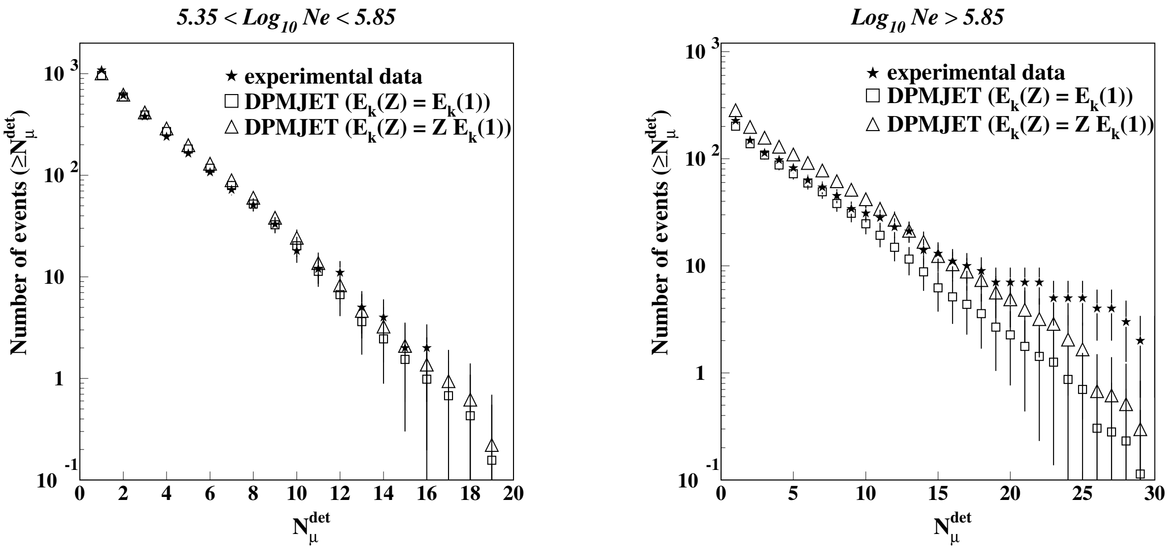

Figure 12: *Multiplicity distributions in MACRO in two intervals of shower size (below and above the knee), for two composition models around the knee:* $Ek(Z) = Ek(1)$ *and* $Ek(Z) = Z * Ek(1)$*. Notice the excellent agreement below the knee.*

3 Interactions and composition

As a first "multicomponent" approach, an analysis is performed by using the observables Ne, $N_\mu{}^{GeV}$, $N_\mu{}^{TeV}$ and $\Delta E_\mu/\Delta L$, as measured by EAS-TOP and LVD ($E_\mu > 1.3$ TeV). To check the "validity" of the observables and the cascade model used, 'very heavy' and 'light' enriched primary beams are selected (from the shower size at EAS-TOP and the muon data in LVD) respectively through: (a) large $N_\mu{}^{TeV}$ muon numbers for $N_e > 2\cdot 10^5$ (which have low probability of being due to fluctuations of light primaries), and (b) large muon energy losses: $\Delta E_\mu/\Delta L > 4\ MeV/cm$ in the highest and lowest LVD counters crossed by the track inside the detector (i.e. high energy/nucleon for $N_e < 2.10^5$). The $Ne - N_\mu{}^{GeV}$ relations at the surface are shown for all events, and the selected ones respectively in figs. 13 and 14. The selected events fall on clearly identified and distinct regions of the chosen parameters. Moreover they fit the expectations from the Dual Parton model of UHE hadronic interactions as implemented in the CORSIKA-HDPM code, for the two classes of primaries.

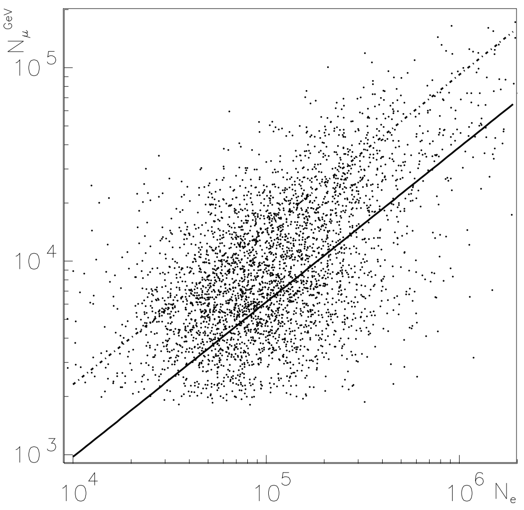

Figure 13: *Experimental* $N_\mu{}^{GeV}$ *vs.* N_e *data. The average predictions of the simulation for Fe (dashed) and proton primaries (solid line) are also shown.*

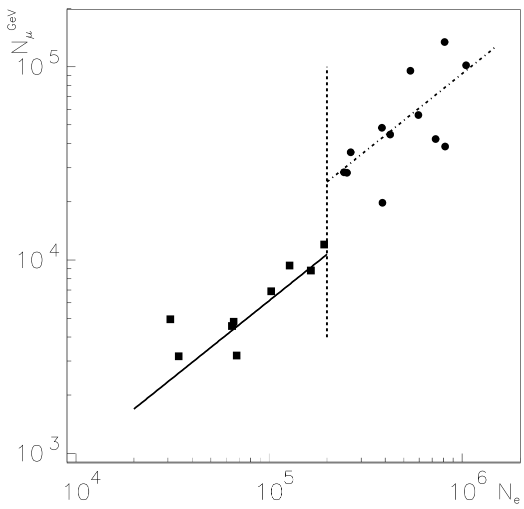

Figure 14: $N_\mu{}^{GeV}$ *vs.* N_e *for selected 'very heavy' and 'light' primaries obtained by applying cuts (a) (circles) and (b) (squares) (see text). For simulated data see fig. 13.*

An identification of individual cosmic ray primaries is thus obtained at Extensive Air Shower energies; and the presence of "iron-like" primaries is proved up to primary energies $E_0 \approx 10^{16}$ eV.

3.1 The secondary production cross section for $x \approx 0.1$

Data on the discrimination of different interaction models from the point of view of the secondary production cross section for $x = E_s/E_0$ values ≈ 1 where reported from the "anticoincidence events" from EAS-TOP and MACRO.

Concerning the secondary production cross section, the interaction models mainly differentiate in the forward region ($x > 0.1$), which is of difficult access to accelerators, mostly for $p-nucleus$ interactions. The energy spectra of different primaries contributing to TeV muons are shown in fig. 15. At primary energies $E_0 \approx 10$ TeV only primary protons contribute. Muon energies can be selected by deep underground detectors (3400 m *w.e.* depth in the case of Gran Sasso laboratories) and, in such range, primary energies can be measured by means of atmospheric Cherenkov light observations.

The contemporaneous measurements of these two quantities provides the unique possibility in ground based cosmic ray experiments of obtaining information on the total energy E_0 and on the minimum energy per nucleon of the primary ($E_\mu^{th} \propto E_0/A$).

The experiment could provide:

a) a measurement of $< N_\mu >$ ($E_\mu \geq 1.3$ TeV) for high energy muons and fixed primary proton energy for $x = E_{sec}/E_0 > 0.1$: since at $E_0 \approx 10$ TeV only proton primaries

contribute to TeV muons, this allows to check the models used in H.E. hadron interactions and represent a significant information for the interpretation of deep underground muon measurements.
b) a study of the p/helium ratio at $30 \leq E_0 \leq 100$ TeV which is quite controversial from direct measurements. Helium primaries contribute to the TeV muons flux above $E_0 \simeq 30$ TeV, carbon primaries above $E_0 \simeq 80$ TeV.

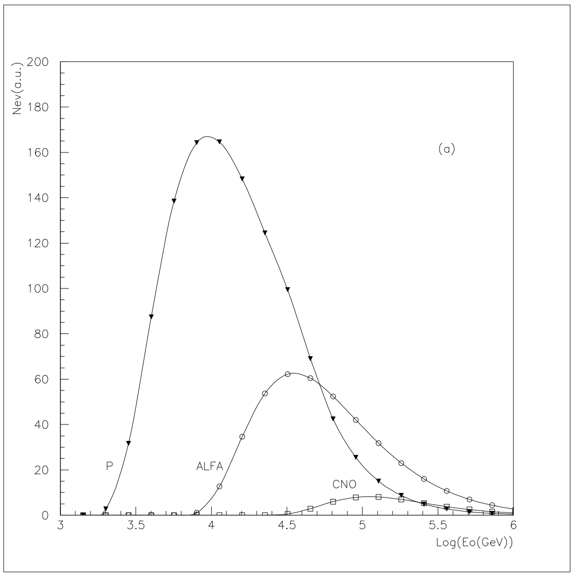

Figure 15: *Energy spectra of primaries contributing to primary muons deep underground (E_μ^{th} = 1.3 TeV, JACEE primary spectra).*

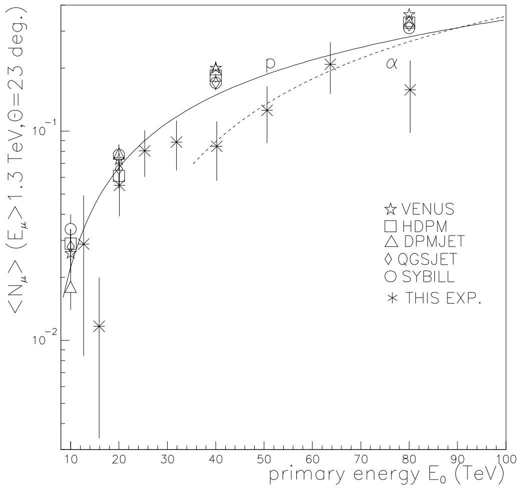

Figure 16: *$< N_\mu >$ measured by the combined operation between the EAS-TOP Cherenkov array and the LVD experiment. The continuous and dotted lines show the results of Forti et al..*

The results of a first run performed in ≈ 100 hours of data taking in coincidence with LVD are shown in fig. 16, together with the results of the calculations by Forti et al. for beams of protons and alfa particles and the expectations from different models and primary protons obtained through the CORSIKA code.
The general trend of expectations over the whole 10 - 100 TeV energy range is confirmed; further statistics (reaching $\approx 10\%$ accuracy) is required.

3.2 The proton interaction length

By selecting EAS near maximum development (for $E_0 = (2-4)10^{15}$ eV) , and generated with high probability by primary protons, through N_e and N_μ, and studying their absorption in the atmosphere, the proton interaction legth is obtained. Such observed value can be directly compared to the expectations from different interaction models (by including in the simulations the full detectors' responses). The experimental data (see tab. 2) are in better agreement with the expectations from "small cross section" models.

Table 2: Observed and simulated interaction lengths $\Lambda_{obs}(g/cm^2)$.

$\log N_e^i$	6.0	6.1	6.2
Exp. Data	75 ± 5	76 ± 6	75 ± 7
He correction	96 ± 6	93 ± 7	86 ± 8
HDPM	90 ± 9	83 ± 9	80 ± 10
VENUS	78 ± 7	72 ± 7	75 ± 10
DPMJET	71 ± 6	66 ± 6	66 ± 7
QGSJET	74 ± 6	69 ± 6	65 ± 7
SIBYLL	105 ± 12	89 ± 10	71 ± 8

4 EAS-TOP References

1 - "The EAS-TOP array at $E_0 = 10^{14} - 10^{16}$ eV : stability and resolutions" *Nucl. Instr. and Methods in Physics Research,* **A277**, *23 (1989)*

2 - "UHE cosmic ray event reconstruction by the electromagnetic detector of EAS-TOP" *Nucl. Instr. and Methods in Physics Research* **A336**, *310 (1993)*

3 - "The hadron calorimeter of EAS-TOP: operation, calibration and resolution" *Nuclear Instruments and Methods in Physics Research A,* **420**, *117 (1999)*

4 - "EAS Cerenkov at Gran Sasso: Correlated Observations at the Surface and with Deep Underground Events" *Il Nuovo Cimento,* **105A**, *12, 1807 (1992)*

5 - "The shapes of the atmospheric Cherenkov light images from extensive air showers" *Astroparticle Physics,* **6**, *143 (1997)*

6 - "Simultaneous observation of extensive air showers and deep underground muons at the Gran Sasso Laboratory" *Physical Review D,* **42**, *1396 (1990)*

7 - "Study of the primary cosmic ray composition around the knee of the energy spectrum" *Physics Letters B,* **337**, *376 (1994)*

8 - "The High Energy Muon Spectrum in Extensive Air Showers: First Data from LVD and EAS-TOP at Gran Sasso" *Astroparticle Physics,* **9**, *185 (1998)*

9 - "Experimental study of hadronic interaction models using coincident data from EAS-TOP and MACRO" *Nuclear Physics B,* **70**, *483 (1999)*

10 - "Identification of light and very heavy cosmic ray primaries at $E_0 \approx 10^{15} eV$ from surface and deep underground measurements at the Gran Sasso Laboratories" *Nuclear Physics B,* **70**, *512 (1999)*

11 - "The EAS Size Spectrum and the Cosmic Ray Energy Spectrum in the Region $10^{15} - 10^{16}$ eV" *Astroparticle Physics,* **10**, *1 (1999)*

12 - "Studies of the Knee in the electron and muon components of Extensive Air Showers at EAS-TOP" *Nuclear Physics B, in press (X ISVHECRI, 1998)*

13 - "A measurement of the solar and sidereal cosmic ray anisotropy at $E_0 \sim 10^{14}$ eV" *The Astrophysical Journal,* **470** *501 (1996)*

14 - "Fractal Behavior of Cosmic Ray Time Series: Chaos or Stochasticity?" *Journal of Geophysical Research,* **98**, *A9, 15,241 (1993)*

15 - "Search for 100 TeV γ-ray emission from the galactic disk" *The Astrophysical Journal,* **397**, *148 (1992)*

16 - "Detection of the UHE Burst from the Crab Nebula on February 23, 1989 from the EAS-TOP array" *Europhysics Letters, 1,* **15**, *81 (1991)*

17 - "Results on candidate UHE Gamma-Ray Sources by the EAS-TOP array (1989-1993)" *Astroparticle Physics,* **3**, *1 (1994)*

18 - "A limit to the rate of Ultra High Energy γ-rays in the primary cosmic radiation" *Astroparticle Physics,* **6**, *71 (1996)*

19 - "Search for Gamma Ray Bursts at photon energies $E \geq 10$ GeV and $E \geq 80$ TeV" *The Astrophysical Journal,* **469**, *305 (1996)*

20 - "The Proton Attenuation Length and the p-air Inelastic Cross Section at $\sqrt{s} \approx 2$ TeV from EAS-TOP" *Nuclear Physics B, in press (X ISVHECRI, 1998)*

21 - "Study of jet production in p-N interactions at $\sqrt{s} \approx 500$ GeV in EAS multicore events" *Nuclear Physics B, in press (X ISVHECRI, 1998)*

22 - "Study of c.r. composition and interaction at $E_0 = 10 - 100$ TeV from the observation of H.E. muons and atmospheric Cherenkov light in EAS" *Nuclear Physics B, in press (X ISVHECRI, 1998)*

23 - "The limit to the UHE extraterrestrial neutrino flux from the observations of Horizontal Air Showers at EAS-TOP" *Physics Letters B* **333**, *555 (1994)*